

See discussions, stats, and author profiles for this publication at: <https://www.researchgate.net/publication/47716838>

Kang, Q., Yang, L., Chen, Y., Luo, S., Wen, L., Cai, Q. & Yao, S. Photoelectrochemical detection of pentachlorophenol with a multiple hybrid CdSexTe_{1-x}/TiO₂ nanotube structure-base...

ARTICLE *in* ANALYTICAL CHEMISTRY · NOVEMBER 2010

Impact Factor: 5.64 · DOI: 10.1021/ac101798t · Source: PubMed

CITATIONS

91

READS

82

7 AUTHORS, INCLUDING:



Qing Kang

National Institute for Materials Science

20 PUBLICATIONS 684 CITATIONS

[SEE PROFILE](#)



Lixia Yang

Lanzhou Jiaotong University

48 PUBLICATIONS 1,767 CITATIONS

[SEE PROFILE](#)

Photoelectrochemical detection of pentachlorophenol with a Multiple Hybrid CdSe_xTe_{1-x}/TiO₂ Nanotube Structure-Based Label-Free Immunosensor

Qing Kang,[†] Lixia Yang,^{†,‡} Yufang Chen,[†] Shenglian Luo,^{*,†,‡} Lingfei Wen,[†] Qingyun Cai,^{*,†} and Shouzhuo Yao[†]

State Key Laboratory of Chemo/Biosensing and Chemometrics, Department of Chemistry, Hunan University, Changsha 410082, P. R. China, and School of Environment and Chemical Engineering, Nanchang Hangkong University, Nanchang 330063, P. R. China

Driven by the urgent demand of detecting trace amounts of pentachlorophenol (PCP) in contaminative water, a label-free immunosensor with ultra sensitivity and high selectivity was constructed based on a hybrid CdSe_xTe_{1-x} ($0 \leq x \leq 1$) nanocrystal (NCs)-modified TiO₂ nanotube (NT) arrays for the first time. The CdSe_xTe_{1-x} NCs were photoelectrodeposited on inner and outer space of the TiO₂ NTs, leading to high photoelectrical conversion efficiency in the visible region. PCP antibodies are covalently conjugated on the TiO₂ NTs due to the large surface area and good biocompatibility. Since the photocurrent is highly dependent on the TiO₂ surface properties, the specific interaction between PCP and the antibodies results in a sensitive change in the photocurrent, with a limit of detection (LOD) of 1 pM. High sensor-to-sensor reproducibility is achieved. The sensor was applied for the direct analysis of river water samples.

Pentachlorophenol (PCP), one of the most commonly environmental pollutants, needs to be monitored due to its adverse effects on human health. PCP enters into environment as byproducts of industrial processes, such as production of antioxidants, dyes, and drugs,¹ the chlorination of drinking water, and the chlorinated bleaching of paper.² It has been classified as priority pollutants by the United States Environmental Protection Agency.³ The concentration level of 1 ppb PCP in drinking water has been defined as the maximum concentration not expected to produce adverse health effects during a lifetime of exposure.⁴ Unfortu-

nately, large-scale use of PCP over the past years has led to the contamination of terrestrial and aquatic ecosystems. It is therefore highly desirable to develop rapid, accurate, and sensitive methods for the detection of trace amounts PCP in environmental samples. Well established methods over the past decades include gas chromatography (GC),⁵ gas chromatography–mass spectrometry (GC-MS),^{6,7} and thin layer chromatography (TLC).^{7,8} Although good sensitivity has been achieved, these protocols are relatively expensive, involve time-consuming sample preparation, and are not suitable for in situ rapid analysis.

The PEC label-free immunoassay is a newly developed analytical method for the rapid and high-throughput biological assay,^{9–11} with the advantages of both label-free immunoassay and PEC method. Compared with the conventional immunoassay method, label-free immunoassay avoids the process of labeling antibody or antigen with makers, saving cost and time.^{11–13} In the PEC process, the light-induced current is used to quantify the target. Benefiting from the separation of excitation source (light) and detection signal (current), some undesired background signals are reduced and high sensitivity are achieved.^{14–16}

However, only a few photoactive materials have been exploited, which limits the development of PEC label-free immunoassay.^{9–11} Anodic TiO₂ NTs grown on Ti foil are with a high surface area

* To whom correspondence should be addressed. E-mail: sllou@hnu.cn (S.L.); qycail0001@hnu.cn (Q.C.).

[†] Hunan University.

[‡] Nanchang Hangkong University.

- (1) Gilman, A.; Douglas, U.; Arbuckle-Sholtz, T.; Jamieson, J. *Chlorophenols and Their Impurities: A Health Hazard Evaluation*; Bureau of Chemical Hazards, Environmental Health Directorate, National Health and Welfare: Ottawa, Ontario, Canada 982, 1989.
- (2) Kristiansen, N. K.; Froshaug, M.; Aune, K. T.; Becher, G.; Lundanes, E. *Environ. Sci. Technol.* **1994**, *28*, 1669–1673.
- (3) Toxic Substance Control Ac; U.S. Environmental Protection Agency: Washington, DC, 1979.
- (4) *Drinking Water Standards and Health Advisories, Summer. 2000*; U.S. Environmental Protection Agency: Washington, DC, 2000.

- (5) Leblance, Y. G.; Gilbert, R.; Hubert, J. *Anal. Chem.* **1999**, *71*, 78–85.
- (6) Mardones, C.; Palma, J.; Sepulveda, C.; Berg, A.; Von Baer, D. *J. Sep. Sci.* **2003**, *26*, 923–926.
- (7) Gremaud, E.; Turesky, R. J. *J. Agric. Food Chem.* **1997**, *45*, 1229–1233.
- (8) Fischer, W.; Bund, O.; Hauck, H. E. *Fresenius J. Anal. Chem.* **1996**, *354*, 889–891.
- (9) Wang, G. L.; Yu, P. P.; Xu, J. J.; Chen, H. Y. *J. Phys. Chem. C* **2009**, *113*, 11142–11148.
- (10) Wang, G. L.; Xua, J. J.; Chen, H. Y.; Fu, S. Z. *Biosens. Bioelectron.* **2009**, *25*, 791–796.
- (11) Haddour, N.; Chauvin, J.; Gondran, C.; Cosnier, S. *J. Am. Chem. Soc.* **2006**, *128*, 9693–9698.
- (12) Floch, F. L.; Ho, H. A.; Leclerc, M. *Anal. Chem.* **2006**, *78*, 4727–4731.
- (13) Kerman, K.; Nagatani, N.; Chikae, M.; Yuhi, T.; Takamura, Y.; Tamiya, E. *Anal. Chem.* **2006**, *78*, 5612–5616.
- (14) Dong, D.; Zheng, D.; Wang, F. Q.; Guo, L. H. *Anal. Chem.* **2004**, *76*, 499–501.
- (15) Liu, S.; Li, C.; Cheng, J.; Zhou, Y. X. *Anal. Chem.* **2006**, *78*, 4722–4726.
- (16) Liang, M. M.; Liu, S. L.; Wei, M. Y.; Guo, L. H. *Anal. Chem.* **2006**, *78*, 621–623.

and high oriented uniform interfacial structure.^{17,18} It has been used as peroxide and hydrogen sensors.^{19,20} It is also a perfect substrate for further electrochemical modification.¹⁷ Its uniform semiconductor interface provides a uniform electric field benefiting the growth on it of semiconductors with fine crystal structure.^{21,22} The wide band gap of TiO₂ limits its direct applications in PEC biosensing since it can only absorbs UV light ($\lambda < 400$ nm) which can kill biomolecules. Modification of TiO₂ with narrow-band gap semiconductors is essential for the PEC biosensing application to enhance the absorption in the visible range and increase the lifetime of charge carriers. CdSe and CdTe are active PEC materials in the visible range and have been successfully used in solar cells.^{23,24} Ternary semiconductor alloy NCs (AB_xC_{1-x})²⁵⁻³⁰ are becoming increasingly important in many areas of nanoscale engineering because of the continuous tenability of their physical and optical properties through gradual variation the composition.

In this work CdSe_xTe_{1-x} (0 ≤ x ≤ 1) NCs were deposited on the inner walls and surface of TiO₂ NTs by photoelectrodeposition. A label-free immunosensor for PCP detection was fabricated using the CdSe_xTe_{1-x} NCs-modified TiO₂ NTs as substrate. High sensitivity was achieved due to the high photoconversion efficiency of CdSe_xTe_{1-x} NCs.

EXPERIMENTAL SECTION

Chemicals and Materials. Titanium foil (≥99.8% purity, 0.127 mm thick) was purchased from Aldrich (Milwaukee, WI). Ethylene glycol, NH₄F, CdSO₄, SeO₂, TeO₂, Na₂S, PCP, trichlorophenol (TCP), and other reagents of analytical reagent grade were all obtained from commercial sources and used as received. Chitosan (CS), glutaraldehyde (GLD), Tween 20, bovine serum albumin (BSA) were purchased from Amresco (U.S.). PCP antibody was obtained from Abcam (U.K.). Phosphate buffer solution (PBS) was prepared with NaHPO₄ and Na₂HPO₄. Twice distilled water was used throughout the experiments.

Fabrication and Characterization of CdSe_xTe_{1-x} (0 ≤ x ≤ 1) NCs-Modified TiO₂ NTs. TiO₂ NTs were prepared by anodization of titanium foils.¹⁸ CdSe_xTe_{1-x} NCs were photoelectrocodeposited on the TiO₂ NTs. The as-prepared materials were characterized by field-emission scanning electron micro-

scope (FE-SEM), High-resolution transmission electron microscopy (HRTEM), energy dispersive X-ray spectrometer (EDS), X-ray diffractometer (XRD), UV-vis diffuse reflectance absorption spectra (DRS), and fluorescence (FL) spectra. The detail is shown in the Supporting Information (SI).

Immunosensor Construction. 50 μL CS solution dissolved in 1% acetic acid was dropped on a CdSe_xTe_{1-x}/TiO₂ NT substrate in a size of 3 cm² and dried at 50 °C. After washing with 0.1 M NaOH and water, the electrode was dipped in 5% GLD solution for 30 min, then rinsed with water to remove the physically adsorbed GLD. 50 μL of 0.5 mg/mL PCP antibody was dropped onto the GLD-activated electrode. After incubating at 4 °C for at least 12 h, the antibody-modified sensor was rinsed with 0.05% Tween 20 solution and then incubated in 3% (w/v) BSA for 1 h to block the unbound sites. The as-prepared sensor was finally rinsed with 0.05% Tween 20. The PEC intensity of the sensor was detected in 0.1 M ascorbic acid (AA) PBS solution after incubating it in a 50 μL of PCP solution at 37 °C for 1 h. All the above-mentioned solutions except the PCP solution were prepared with 0.01 M PBS (pH 7.4).

PEC Activity Determination. PEC activity was determined in 0.6 M Na₂S solution using a CHI electrochemical analyzer (CHI660C, Shanghai Chenhua Instrument Co. Ltd.) in a standard three-electrode system. The incident light intensity through a UV cut filter from a 300 W Xe lamp was 100 mW cm⁻² measured by a radiometer (OPHIR, Littleton, CO). PEC immunoassay was performed in 0.1 M pH 7.0 PBS containing ascorbic acid (AA) as oxidative quencher.

RESULTS AND DISCUSSIONS

Characterization. The prepared TiO₂ NTs have an average length of 6.5 μm and inner diameter of ~70 nm (the SEM not shown). The presence of well-aligned NTs vertically oriented from the Ti foil substrate not only provides accessible accesses for depositing high concentration of sensitizing NCs, but promotes the directional charge transport due to the one-dimensional features of the tubes.²² FE-SEM images (SI Figure S1) reveals that CdSe_{0.75}Te_{0.25} NCs in an average size of 56 nm are deposited on both the surface and inside of the TiO₂ NTs, while the CdTe and CdSe NCs are mainly distributed on the surface due to their large particle size (~110 nm). EDS analysis shows that the atom ratio of Cd: (Se + Te) is not strictly in accordance with 1:1 due to the low pH of plating solution (SI Table S1).³¹ The ratio of Se:Te is also not in accordance with the molar ratio of HSeO₂⁺:HTeO₂⁺ in solution. More Se was deposited due to the higher reactivity of HSeO₂⁺ with respect to HTeO₂⁺.²⁶ XRD spectra (SI Figure S2A) reveals that the pure TiO₂ NTs are in anatase phase, while the CdSe_{0.75}Te_{0.25} NCs are in a mixture of hexagonal and cubic phases which are further confirmed by HRTEM and electron diffraction pattern (SI Figure S2B). CdSe_{0.75}Te_{0.25} NCs appeared on TEM grids are homogeneous NCs instead of gradient NCs, which is expected to exhibit significant photoactivity and optical bowing effects.²⁷

PEC Behavior of CdSe_xTe_{1-x}/TiO₂ NTs. As a PEC sensor, high photoelectrical activity is essential to achieving a high sensitivity. As shown in Figure 1A, the unmodified TiO₂ NTs show a week response, while the CdSe_xTe_{1-x}/TiO₂ NTs show high

- (17) Grimes, C. A.; Mor, G. K. *TiO₂ Nanotube Arrays: Synthesis, Properties, and Applications*; Springer: Berlin, 2009.
- (18) Wang, D. A.; Yu, B.; Wang, C. W.; Zhou, F.; Liu, W. M. *Adv. Mater.* **2009**, *21*, 1–4.
- (19) Chen, D.; Zhang, H.; Li, X.; Li, J. H. *Anal. Chem.* **2010**, *82*, 2253–2261.
- (20) Varghese, O. K.; Mor, G. K.; Grimes, C. A.; Paulose, M.; Mukherjee, N. J. *Nanosci. Nanotechnol.* **2004**, *4*, 733–737.
- (21) Yang, L. X.; Luo, S. L.; Liu, R. H.; Cai, Q. Y.; Xiao, Y.; Liu, S. H.; Su, F.; Wen, L. H. *J. Phys. Chem. C* **2010**, *114*, 4783–4789.
- (22) Zhang, H.; Quan, X.; Chen, S.; Yu, H. T.; Ma, N. *Chem. Mater.* **2009**, *21*, 3090–3095.
- (23) Nestor, G.; Teresa, L. V.; Iva'n, M. S.; Juan, B.; Roberto, G. *J. Phys. Chem. C* **2009**, *113*, 4208–4214.
- (24) Gao, X. F.; Li, H. B.; Sun, W. T.; Chen, Q.; Tang, F. Q.; Peng, L. M. *J. Phys. Chem. C* **2009**, *113*, 7531–7535.
- (25) Gurusinghe, N. P.; Hewa-Kasakarage, N. N.; Zamkov, M. *J. Phys. Chem. C* **2008**, *112*, 12795–12800.
- (26) Piven, N.; Susha, A. S.; Doblinger, M.; Rogach, A. L. *J. Phys. Chem. C* **2008**, *112*, 15253–15259.
- (27) Bailey, R. E.; Nie, S. M. *J. Am. Chem. Soc.* **2003**, *125*, 7100–7106.
- (28) Muthukumarasamy, N.; Jayakumar, S.; Kannan, M. D.; Balasundaraprabhu, R. *Solar Energy* **2009**, *83*, 522–526.
- (29) Wei, S. H.; Zhang, S. B.; Zunger, A. *J. Appl. Phys.* **2000**, *87*, 1304–1311.
- (30) Bernard, J. E.; Zunger, A. *Phys. Rev. B* **1986**, *34*, 5992–5995.

- (31) Peng, X. S.; Zhang, J.; Wang, X. F.; Wang, Y. W.; Zhao, L. X.; Meng, G. W.; Zhang, L. D. *Chem. Phys. Lett.* **2001**, *343*, 470–474.

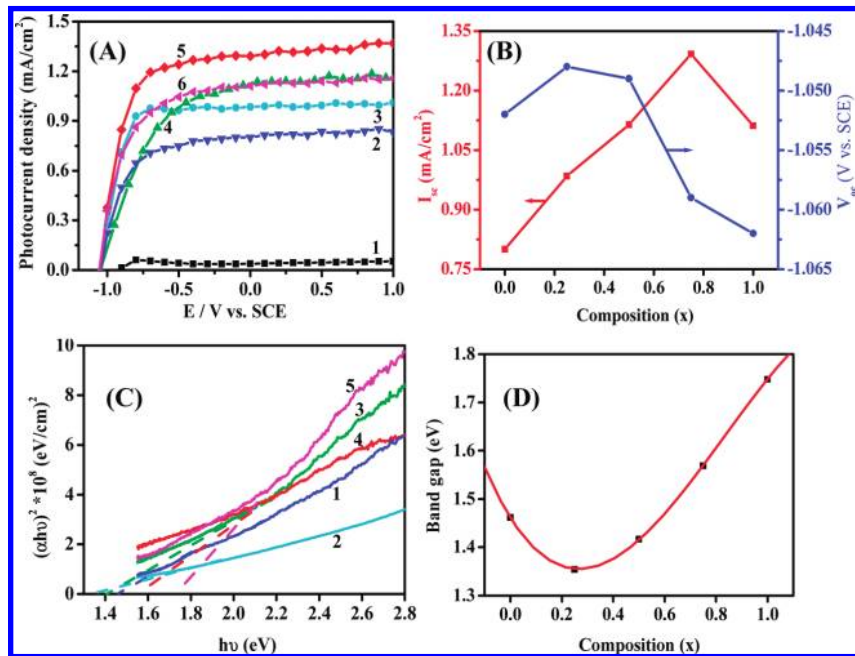


Figure 1. (A) Photocurrent response of pure TiO_2 NTs (curve 1) and $\text{CdSe}_x\text{Te}_{1-x}/\text{TiO}_2$ NTs at compositions of $x = 0, 0.25, 0.5, 0.75$, and 1 for curves 2–6. (B) Effect of composition x on open circuit voltage and short circuit current density for $\text{CdSe}_x\text{Te}_{1-x}/\text{TiO}_2$ NT electrode. (C) $(\alpha h\nu)^2$ versus $h\nu$ plots of $\text{CdSe}_x\text{Te}_{1-x}/\text{TiO}_2$ NTs at compositions of $x = 0, 0.25, 0.5, 0.75$, and 1 for curve 1–5. (D) Various of the band gap energy of $\text{CdSe}_x\text{Te}_{1-x}/\text{TiO}_2$ NTs versus the composition coefficient (x).

photocurrent responses, with the photocurrent depending on the alloy composition. The highest photoactivity is observed on the $\text{CdSe}_{0.75}\text{Te}_{0.25}/\text{TiO}_2$ NTs. The modification of $\text{CdSe}_x\text{Te}_{1-x}$ NCs results in a significant increase in the absorption in visible region, allowing efficient light harvesting.

The short circuit current (I_{sc}) of the $\text{CdSe}_{0.75}\text{Te}_{0.25}/\text{TiO}_2$ NTs is much higher than that of the CdSe or CdTe-deposited TiO_2 NTs (Figure 1B), with I_{sc} of 1.29 ($\text{CdSe}_{0.75}\text{Te}_{0.25}$), 0.80 (CdTe), and 1.11 mA/cm^2 (CdSe), respectively. The open circuit potential (V_{oc}) of $\text{CdSe}_x\text{Te}_{1-x}/\text{TiO}_2$ NT electrode is around -1.05 V which is more negative than that ($V_{oc} \approx -0.91$ V) of TiO_2 NT electrode (Figure 1A), demonstrating that the coupling between TiO_2 and $\text{CdSe}_x\text{Te}_{1-x}$ shifts the Fermi level to more negative potential. The more negative V_{oc} means the more effective separation of photogenerated pairs. In the case of $\text{CdSe}_x\text{Te}_{1-x}/\text{TiO}_2$ NTs, the V_{oc} slightly decreases with increasing the Se content (Figure 1B).

The optical properties of the $\text{CdSe}_x\text{Te}_{1-x}/\text{TiO}_2$ NTs within 300–800 nm was further investigated by measuring the UV–vis DRS of the $\text{CdSe}_x\text{Te}_{1-x}/\text{TiO}_2$ NTs. For allowed band gap electronic transitions, the absorption coefficient is given by^{28,29}

$$\alpha = A(h\nu - Eg)^{0.5}/h\nu$$

Where A is a constant, h the Planck's constant, and ν the frequency of the incident light. Shown as in Figure 1C, the linear plots of $(\alpha h\nu)^2$ versus $h\nu$ indicate that the semiconductors are direct band gap materials. The intercept on the abscissa at $\alpha = 0$ gives the band gap (Eg) of $\text{CdSe}_x\text{Te}_{1-x}$. Figure 1D shows the composition (x)-dependent Eg . Eg varies from 1.46 eV (CdTe/ TiO_2 NTs) to 1.75 eV (CdSe/ TiO_2 NTs), with the minimum (1.35 eV) observed at $x = 0.25$. The nonlinearity of Eg - x plots is measured with a so-called bowing coefficient b :

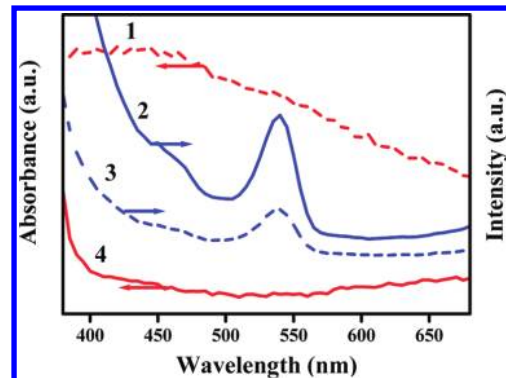


Figure 2. UV–vis DRS (line 1, 4) and FL spectra (line 2, 3) of pure TiO_2 NTs (line 2, 4) and $\text{CdSe}_{0.75}\text{Te}_{0.25}/\text{TiO}_2$ NTs (line 1, 3).

$$Eg(\text{CdSe}_x\text{Te}_{1-x}) = xEg(\text{CdSe}) + (1-x)Eg(\text{CdTe}) - bx(1-x)$$

The bowing effect is associated with a large lattice mismatch between binary subcompounds and differences in atomic radii and electronegativities of alloying elements, and matches well with the bowing nature of cation semiconductor alloy ($\text{AB}_x\text{C}_{1-x}$) NCs modeled by Zunger.³⁰ The significant bowing effect indicates that even a small amount of Te in CdSe or Se in CdTe can drastically reduce its band gap. SI Table S2 lists the band gap and bowing coefficient of $\text{CdSe}_x\text{Te}_{1-x}/\text{TiO}_2$ NTs as the function of the composition.

The optical properties of $\text{CdSe}_{0.75}\text{Te}_{0.25}/\text{TiO}_2$ NTs were further characterized by UV–vis DRS and FL spectra. Figure 2 shows that the modification of $\text{CdSe}_{0.75}\text{Te}_{0.25}$ results in a significant enhancement in absorption in visible range (line 1 versus line 4), and a decrease in FL intensity at 540 nm (line 2 versus line 3). The strong FL peak at 540 nm and weak shoulder at ~ 466 nm are attributed to the formation of oxygen vacancies at the TiO_2 NT surface.^{32,33} The photogenerated hole and electron pairs

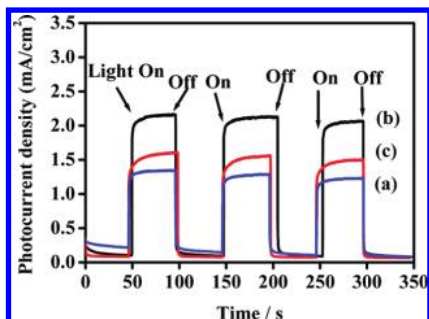


Figure 3. Photocurrent responses of $\text{CdSe}_{0.75}\text{Te}_{0.25}/\text{TiO}_2$ NT electrodes with deposition time of 1 h (a), 2 h (b), and 4 h (c).

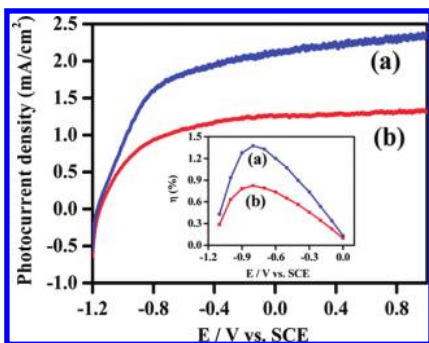


Figure 4. Comparison of PEC performances of $\text{CdSe}_{0.75}\text{Te}_{0.25}/\text{TiO}_2$ NT electrodes prepared by (a) photoelectrodeposition and (b) electrodeposition. The inset is the corresponding photoconversion efficiencies.

are recombined at the oxygen vacancies resulting in FL. The lower FL intensity of $\text{CdSe}_{0.75}\text{Te}_{0.25}/\text{TiO}_2$ NTs suggests a lower density of recombination centers (surface states), and consequently longer lifetime of photogenerated carriers resulted from the introduction of $\text{CdSe}_{0.75}\text{Te}_{0.25}$. Similar results have been reported for $\text{TiO}_2/\text{Carbon nanotube composites}^{32}$ and ZnFe_2O_4 modified TiO_2 NTs.³³

Figure 3 shows the photocurrent response of TiO_2 NTs loaded with different mass of $\text{CdSe}_{0.75}\text{Te}_{0.25}$ NCs. The electrode responds promptly to light on/off. The 2 h deposition of $\text{CdSe}_{0.75}\text{Te}_{0.25}$ achieves the highest photocurrent. Longer deposition time over than 2 h (Line c in Figure 3) leads to overcast of $\text{CdSe}_{0.75}\text{Te}_{0.25}$ NCs, which may block the TiO_2 NTs resulting in a decrease in the surface area and consequently photocurrent.

It is noteworthy to point out that the photocurrent is also dependent on the deposition method of $\text{CdSe}_{0.75}\text{Te}_{0.25}$ NCs. Shown in Figure 4A, as compared with electrodeposition, the photoelectrodeposition achieves 2-fold higher photocurrent, and more difficult saturation of photocurrent, suggesting the superior electron transfer efficiency resulted from photoelectrodeposition. The inset shows the corresponding photoconversion efficiency calculated using the following equation:^{34,35}

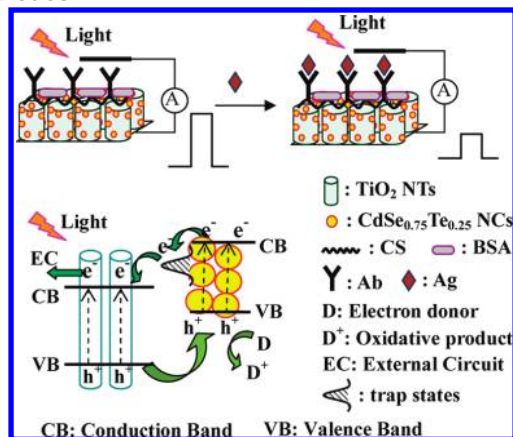
$$\eta(\%) = [(\text{total power output} - \text{electrical power input}) / \text{light power input}] \times 100 = j_p [(E_{\text{rev}}^0 - |E_{\text{app}}|) / I_0] \times 100$$

where j_p is the photocurrent density in mA/cm^2 , E_{rev}^0 the standard reversible potential which is 1.23 V_{NHE}, and E_{app} the

(32) Yao, Y.; Li, G. H.; Ciston, S.; Lueptow, R. M.; Gray, K. A. *Environ. Sci. Technol.* **2008**, *42*, 4952–4957.

(33) Hou, Y.; Li, X. Y.; Zhao, Q. D.; Quan, X.; Chen, G. H. *Adv. Funct. Mater.* **2010**, *20*, 2165–2174.

Scheme 1. Scheme Diagram of the Immunosensor Construction and Ideal Stepwise Band Edge Structures for Efficient Transport of the Excited Electrons and Holes in $\text{CdSe}_{0.75}\text{Te}_{0.25}/\text{TiO}_2$ NT Electrodes



applied potential, I_0 the power density of incident light (100 mW/cm²).

The highest photoconversion efficiency observed on the photoelectrodeposited $\text{CdSe}_{0.75}\text{Te}_{0.25}/\text{TiO}_2$ NTs is 1.67 times that on electrodeposited $\text{CdSe}_{0.75}\text{Te}_{0.25}/\text{TiO}_2$ NTs. The higher photoconversion efficiency can be ascribed to the higher deposition efficiency of photoelectrodeposition at a given applied potential, resulting in the formation of more NCs. Under illumination, the photogenerated charges are highly active in the formation of NCs.

Performance of the Immunosensor. Due to the high photoelectroconversion efficiency, the $\text{CdSe}_{0.75}\text{Te}_{0.25}/\text{TiO}_2$ NTs prepared by photoelectrodeposition were used as the substrate of the PEC biosensor. Scheme 1 presents a model energy scheme of $\text{CdSe}_{0.75}\text{Te}_{0.25}/\text{TiO}_2$ NTs containing a Te impurity-induced trap state within the band gap of CdSe. In contrast to the double step band-edge in CdSe/TiO_2 NTs or CdTe/TiO_2 NTs, the triple stepwise band-edge structure built in the $\text{CdSe}_{0.75}\text{Te}_{0.25}/\text{TiO}_2$ NTs is advantageous to the electron injection and hole recovery of the system, which is responsible for the high photocurrent in the $\text{CdSe}_{0.75}\text{Te}_{0.25}/\text{TiO}_2$ NT electrodes.³⁶ Since the conduction band (CB) level of TiO_2 lies more positive than the CB level and trap state of $\text{CdSe}_{0.75}\text{Te}_{0.25}$, photogenerated electrons coming from the $\text{CdSe}_{0.75}\text{Te}_{0.25}$ are ready to inject into the CB of TiO_2 , and flow to the external circuit through the conductive Ti substrate. Simultaneously, holes in TiO_2 valence band (VB) transfer to $\text{CdSe}_{0.75}\text{Te}_{0.25}$ VB, accumulate there, and are consumed by participating in oxidation. The different transfer paths of electrons and holes lead to a high photoelectrocatalytic efficiency. With the immunoreaction between PCP and the antibody modified on the $\text{CdSe}_{0.75}\text{Te}_{0.25}/\text{TiO}_2$ NTs, immunocomplex was formed, resulting in an increase in the steric hindrance toward the diffusion of quencher molecules and/or photogenerated holes on the electrode interface, and consequently a decrease in photocurrent.

(34) Ruan, C.; Paulose, M.; Varghese, O. K.; Grimes, C. A. *Sol. Energy Mater. Sol. Cells* **2006**, *90*, 1283–1295.

(35) Mohapatra, S. K.; Raja, K. S.; Mahajan, V. K.; Misra, M. *J. Phys. Chem. C* **2008**, *112*, 11007–11012.

(36) Franzl, T.; Muller, J.; Klar, T. A.; Rogach, A. L.; Feldmann, J. *J. Phys. Chem. C* **2007**, *111*, 2974–2979.

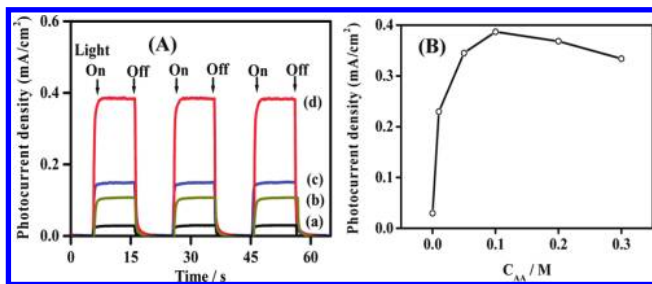


Figure 5. (A) Photocurrent response of $\text{CdSe}_{0.75}\text{Te}_{0.25}/\text{TiO}_2$ NTs in different solutions: 0.1 M PBS (pH 7.0) alone (a); 0.1 M glutathione in PBS (b); saturated uric acid in PBS (c); and 0.1 M AA in PBS (d). (B) AA concentration-dependent photocurrent response in 0.1 M PBS (pH 7.0).

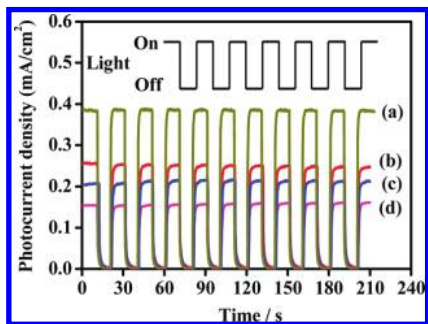


Figure 6. Photocurrent response of $\text{CdSe}_{0.75}\text{Te}_{0.25}/\text{TiO}_2$ NT electrodes in the presence of AA (0.1 M) in 0.1 M PBS (pH 7.0): (a) before and (b) after antibody immobilization; (c) after further anchoring BSA; and (d) after incubation with the corresponding 0.3 mM PCP.

In order to obtain high and stable photocurrent, electron donors (or oxidative quenchers) are necessary. An efficient electron donor can capture the hole of the semiconductor, suppressing the electron–hole recombination and therefore enhancing the photocurrent intensity. Although Na_2S is widely used as electron donor in strong alkaline solution (around pH 12), a mild pH solution is strongly required in biosensing. Antioxidants including uric acid, glutathione, and AA were investigated as electron donor with results shown in Figure 5A. The highest photocurrent is achieved in AA solution. The photocurrent increases with increasing AA concentration up to 0.1 M, and then decreases (Figure 5B). The decrease in photocurrent at high AA concentration can be ascribed to the absorbance of the quencher solution, which thus decreases the irradiation intensity and efficiency of excited electron–hole center formation.^{9,10}

Direct label-free detection is with many advantages such as saving time and expense.^{11,13,37} In this work, a label-free immunosensor was fabricated by successive modifying the $\text{CdSe}_{0.75}\text{Te}_{0.25}/\text{TiO}_2$ NTs with anti-PCP Ab and BSA. The corresponding modification-induced changes in photocurrent are shown in Figure 6. As expected, the successive binding of Ab and BSA on the $\text{CdSe}_{0.75}\text{Te}_{0.25}/\text{TiO}_2$ NTs induces significant decreases in photocurrent. Such decreases in photocurrent are ascribed to the modification-induced steric hindrances toward the diffusion of quencher molecules and/or photogenerated holes on the electrode interface. The specific immunoreaction between PCP and the antibody results in a further 25% decrease in the

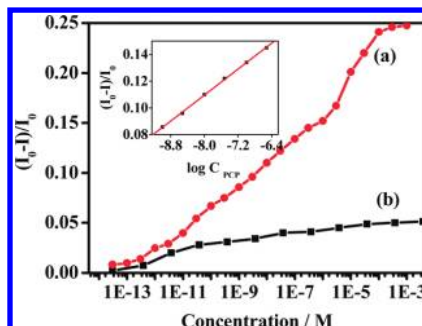


Figure 7. Calibration curves for photoelectrochemical immunosensor for (a) PCP determination and the responses of the immunosensor for (b) TCP.

photocurrent intensity. Control experiment carried out in PBS solution without PCP at 37 °C for 1 h shows no apparent changes in photocurrent intensity. As shown in Figure 6, the sensor shows reproducible photocurrent responses, with no decrease in repeated irradiations of more than 10 times.

The decrease in photocurrent is dependent on the PCP concentration as Figure 7 a. The normalized photocurrent response gradually increases with increasing PCP concentrations and ultimately leveled off at the concentration of higher than 0.1 mM. The relative change of photocurrent is linear proportional to the logarithm of PCP concentrations in the ranges of 1 nM to 0.3 μM as shown in the inset of Figure 7, with a correlation coefficient of 0.999, and a limit of detection (LOD) of 1 pM calculated based on the response of three times the standard deviation of zero-dose response ($n = 15$). The achieved LOD is low enough to measure PCP residues in water samples, and much lower than the published values. A few examples are cited here: Gremaud et al.⁷ choose three methods to detect PCP in wood. The LOD approach 50 ppb (0.187 μM) by GC-MS and 1 ppm (3.75 μM) by TLC when 100 mg of wood was used for analysis and 1 ppm (3.75 μM) for the colorimetric method when 1 g of wood was used for detection. Crespilho et al.³⁸ developed a humic acid-based poly(allylamine hydrochloride) sensor for PCP detection with a LOD of 1 nM. Saby et al.³⁹ combined chemical and electrochemical approach using bis(trifluoroacetoxy)iodobenzene and glucose oxidase for the detection of chlorinated phenols with a LOD of 4 nM. Wang et al.⁴⁰ applied Mn-doped ZnS quantum dots for the room-temperature phosphorescence optosensing of PCP with a LOD of 86 nM.

The specificity of the PCP immunosensor was investigated by measuring the sensor responses to TCP, an analog of PCP. As shown in Figure 7 b, the normalized photocurrent response to TCP is markedly lower than to PCP.

The reproducibility of the immunosensor was evaluated by intra-assay and interassay relative standard deviation (RSD). A 50 μM PCP solution was repeatedly determined using the immunosensor for six times, giving an intra-assay RSD of 6.24%. The interassay RSD on seven immunosensor is 7.19%. The results indicate a good reproducibility of the fabrication protocol.

The long-term storage stability of the immunosensor was investigated by storing the immunosensor in 0.1 M PBS at 4 °C

(38) Crespilho, F. N.; Zucolotto, V.; Siqueira, J. R., Jr.; Constantino, C. J. L.; Nart, F. C.; Oliveira, O. N., Jr. *Environ. Sci. Technol.* 2005, 39, 5385–5389.

(39) Saby, C.; Male, K. B.; Luong, J. H. T. *Anal. Chem.* 1997, 69, 4324–4330.

(40) Wang, H. F.; He, Y.; Ji, T. R.; Yan, X. P. *Anal. Chem.* 2009, 81, 1615–1621.

over two weeks; the immunosensor still retained 91.31% of the initial response. The good stability of the immunosensor is attributed to that anti-PCP is firmly cross-linked to the sensor surface through chitosan, a good biocompatible material which is favorable to retaining the biological activity of the immobilized antibody.¹⁰

PCP Assay in Water Samples. In order to ascertain the potential applications of the sensor, water samples collected from Xiangjiang River, a local river, was analyzed. After being filtered with 0.45 μm cellulose membranes, the samples were directly analyzed. Total amount of PCP in the water sample was estimated to be 2.35 nM. The water sample was also analyzed by ECL method (data not shown). The ECL result is 1.79 nM which is consistent with the proposed method. Aim to establish the suitability of the proposed method, known amounts of the standard PCP were added into the water sample. The recovery ranges from 98.5% to 102.4%, indicating that this method can be used in real sample analysis.

CONCLUSION

Multiple hybrid $\text{CdSe}_x\text{Te}_{1-x}/\text{TiO}_2$ NT photoelectrodes were fabricated by photoelectrodeposition of $\text{CdSe}_x\text{Te}_{1-x}$ on TiO_2 NTs. Using photoelectrodeposition, higher photocurrent was achieved as compared with electrodeposition. The ternary hybrid $\text{CdSe}_x\text{Te}_{1-x}$ NCs show higher photoconversion efficiency as compared with binary hybrid CdSe or CdTe NCs. The photoconversion efficiency is dependent on the NC composi-

tion, and the highest photoconversion efficiency of 1.37% under visible light irradiation is observed for the $\text{CdSe}_{0.75}\text{Te}_{0.25}/\text{TiO}_2$ NT electrode. A label-free, highly selective and ultra sensitive PEC immunosensor for PCP was fabricated by successive modifying the $\text{CdSe}_{0.75}\text{Te}_{0.25}/\text{TiO}_2$ NT electrode with anti-PCP Ab and BSA. PCP was quantified by measuring the photocurrent intensity. A limit of recognition (LOR) of 1 pM is achieved. Such a novel, label-free PEC immunosensor opened a new perspective for the application of semiconductors in analytical field.

ACKNOWLEDGMENT

Support of this work by the National Basic Research Program of China (Grants No. 2009CB421601), the National Science Foundation of China (Grant Nos. 20775024, 50878079, and 51008149), and the National Science Foundation for Distinguished Young Scholars (Grant No. 50725825) are gratefully acknowledged.

SUPPORTING INFORMATION AVAILABLE

Additional information including Figures S1–S3 and Tables S1 and S2. This material is available free of charge via the Internet at <http://pubs.acs.org>.

Received for review July 15, 2010. Accepted October 26, 2010.

AC101798T